Available online www.jsaer.com

***Journal of Scientific and Engineering Research*, 2020, 7(10):14-24**

Research Article

ISSN: 2394-2630
CODEN(USA): JSERBR

3D Modelling Study of a Silicon Solar Cell: Effect of Doping Rate and Grain Size

Moussa Camara[1,2], Mamadou Lamine BA[1], Gora Diop[1], Amadou Mamour BA[1], Ibrahima Diatta[1], Moustapha Thiame[1,2], Gregoire Sissoko[1]*

[1]Laboratory of Semiconductors and Solar Energy, Physics Department, Faculty of Science and Technology, University Cheikh Anta Diop, Dakar, Senegal
[2]Laboratory of Chemistry and Physics of Materials (LCPM), Assane Seck University of Ziguinchor, Ziguinchor, Senegal
***e-mail: gsissoko@yahoo.com**

Abstract In this article, we have highlighted the influence of doping rate and grain size on the excess minority carrier's density in the base. From the expression of the continuity equation describing diffusion phenomena and the recombination mechanisms in the bulk as on surfaces, we have determined the expression of the minority carrier's density in the base according to the doping rate of the base and the grain size. The objective of this work is to determine the effect of the doping rate on the excess minority carrier's density for different grain sizes. The profile of the minority carriers density according to the doping rate, for different values of grain size, allowed us to deduce the optimal doping rate (Nbopt) corresponding to the maximum of the excess minority carrier's density of improved carriers (δnmax) in open-circuit in the moderate base doping (10^{15} $cm^{-3} \leq Nb \leq 10^{17}$ cm^{-3}), depending on the grain size.

Keywords Solar cell, Doping Rate, Grain Size, Minority Carrier Density

1. Introduction

Several studies [1] have been carried out to study the external influence on the electrical parameters of a solar cell, such as: magnetic field [2], temperature [3, 4, 5], both magnetic field and temperature combined [3, 4, 5], electric field [6, 7], irradiation energy flow [8,9,10], sun concentration [11], and incidence angle [12]. Studies have also made it possible to highlight the influence of internal parameters such as: base thickness [13], doping rate [14, 15], minority carriers diffusion coefficient [16], lifetime [17], diffusion length [18], grain size [19, 20, 21], surface recombination velocity at junction [19, 20, 21], at rear side [19, 20, 21] and at interfaces (Sg) [19, 20, 21], on the quality of the solar cell. Thus the recent advances in research on photovoltaic devices have led to solar cells with efficiency greater than 20% [22,23].

This efficiency depends on excess minority carrier density recombination parameters such as, diffusion length and recombination velocities at the junction and the interfaces [19]. The diffusion length is limited by different impurities whose doping rate. So, it is great interest to know the effect of doping level on the cell efficiency before the cell fabrication

The effects of the base's doping rate have been analyzed in many works and some approaches are recently used to determine the optimum base's thickness according to the base's doping rate [15].

The objective of this work is to make a contribution in understanding the behavior of polycrystalline solar cell under the doping level effect, for different grain sizes.

The optimal doping rate of the base, corresponding to the maximum of excess minority carriers density is determined according to the grain size.

2. Theoretical Study

2.1. Description of the Solar Cell

In our study, we selected the three-dimensional mathematical model (Figure 1) [19]. The solar cell type is n^+- p-p^+[19]. It is illuminated by its front side and the junction of the solar cell will be taken as the origin of the z axis, the center of the junction will be considered the origin of the (xoy) landmark (Figure 1). We assume in our modelling that all the grains have a columnar form [6, 20, 21, 24, 25, 26] and have the same size as shown in Figure1. We will overlook the existing crystalline field in the base [21] and the emitter contribution to the photocurrent [19]. The illumination is uniform, so we have a generation rate depending solely on the depth z in the base [26, 27, 28]. The front side that receives the radiation is covered with an anti-reflective coating [29]. Grain boundaries are perpendicular to the junction [19, 26, 30] and their recombination velocities are independent of the generation rate. So the boundary conditions of the continuity equation are linear [19].

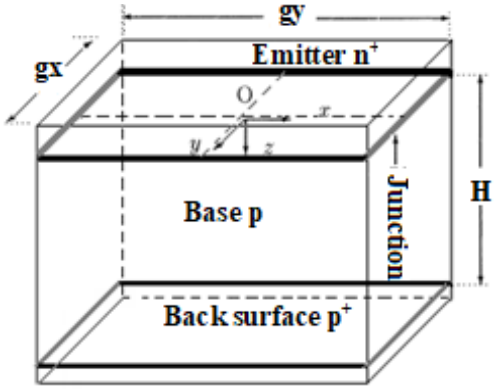

Figure 1: Pattern of a silicon grain of the solar cell

2.2. Continuity Equation

The density of minority carriers in the base is governed by the continuity equation describing diffusion phenomena and recombination mechanisms in bulk and interfaces.

This continuity equation of photogenerated minority carriers' is generally given by the following relationship:

$$\frac{1}{e}\nabla J - R + G = \frac{\partial \delta n(x,y,z)}{\partial t} \quad (1)$$

G(z) is the generation rate, given by [22]:

$$G(z) = \sum_{i=1}^{3} a_i \cdot \exp(-b_i \cdot z) \quad (2)$$

The a_i and b_i coefficients are obtained from the tabulated values of solar illumination and the dependence of the silicon absorption coefficient with the wavelength [31, 32],

z is the depth of the solar cell base, illuminated by the front side.

$$R = \frac{\delta n(x,y,z)}{\tau(Nb)} \quad (3)$$

R is the recombination rate, and $\tau(N_B)$ is the lifetime of minority carriers in the base, which depends on the doping rate of the base, [33,34]:

$$\tau(Nb) = \frac{12}{1 + \frac{Nb}{5 \cdot 10^{16}}} \quad (4)$$

J is the current density, given by:

$$J = J_c + J_d = e \cdot \mu \cdot E \cdot \delta n(x,y,z) + e \cdot Dn(Nb) \cdot \nabla \delta n(x,y,z) \quad (5)$$

Dn(Nb) is the electron diffusion coefficient in the base, as a function of the doping rate of the base. Its expression is given by [33, 34**]**

$$Dn(Nb) = \frac{1350 \cdot V_T}{\sqrt{1 + 81 \cdot \frac{Nb}{Nb + 3.2 \cdot 10^{18}}}} \quad (6)$$

Nb is the doping rate of the base,

δn (x, y, z) is the excess minority carriers density in the base of the solar cell.

J_c is the conduction current density and J_d is the diffusion current density.

Thus, the equation (5) becomes:

$$J = e \cdot Dn(Nb) \cdot \nabla \delta n(x, y, z) \quad (7)$$

The equation (1) becomes:

$$\frac{1}{e} \nabla \left(e \cdot Dn(Nb) \cdot \delta n(x, y, z)\right) - \frac{\partial \delta n(x, y, z)}{\tau(Nb)} + G(z) = \frac{\partial \delta n(x, y, z)}{\partial t} \quad (8)$$

In static regime, we have:

$$\frac{\partial \delta n(x, y, z)}{\partial t} = 0 \quad (9)$$

The continuity equation (8) then becomes

$$\frac{\partial^2 \delta n(x, y, z)}{\partial x^2} + \frac{\partial^2 \delta n(x, y, z)}{\partial y^2} + \frac{\partial^2 \delta n(x, y, z)}{\partial z^2} - \frac{\delta n(x, y, z)}{Ln(Nb)^2} = -\frac{G(z)}{Dn(Nb)} \quad (10)$$

$Ln(N_B)$ is the electrons diffusion length in the base that depends on the doping rate of the base:

$$Ln(Nb) = \sqrt{Dn(Nb) \cdot \tau(Nb)} \quad (11)$$

G (z) is the generation rate at depth z.

To solve the continuity equation (9), we will use solutions such as [19, 20, 21, 26, 35]

$$\delta n(x, y, z) = \sum_k \sum_j Zkj(z) \cdot \cos(C_k \cdot x) \cdot \cos(C_j \cdot y) \quad (12)$$

With $$Zkj(z) = A_{kj} \cdot \cosh\left(\frac{z}{L_{kj}}\right) + B_{kj} \cdot \sinh\left(\frac{z}{L_{kj}}\right) - \sum_{i=1}^{n} K_i \cdot \exp - b_i \cdot z \quad (13)$$

$$K_i = \frac{a_i \cdot L_{kj}^2}{D_{kj} \cdot \left(b_i^2 \cdot L_{kj}^2 - 1\right)} \quad (14)$$

Akj and Bkj will be determined from the boundary conditions at the emitter-base junction and the rear face [19, 20, 21, 35, 36] that will be given below:

- At the emitter-Base junction

$$Dn(Nb) \cdot \left(\frac{\partial \delta n(x, y, z)}{\partial z}\right)_{z=0} = S_f \cdot \delta n(x, y, 0) \quad (15)$$

Sf is the recombination velocity at the junction. It is the flow of minority carriers that crosses the junction. It is the sum of two terms ($S_f = S_{f0} + S_{fj}$) [37]: S_{f0} is the speed of intrinsic recombination at the junction induced by shunt resistance. It is related to carriers lost at the junction due to traps and recombination sites in this area. And S_{fj} translates the current flow imposed by the external load and it defines the operating point of the solar cell by providing information on the density of minority carriers that have successfully crossed the junction [19, 36, 38].

- In back face.

$$Dn(Nb)\cdot\left(\frac{\partial\delta n(x,y,z)}{\partial z}\right)_{z=H} = -S_b\cdot\delta n(x,y,H) \quad (16)$$

S_b is the back surface recombination velocity. It quantifies the rate of excess minority carriers effectively lost by recombination, at the back surface of the cell [19, 36, 39].

- At grain boundaries:

The boundary conditions properly are given by the equations (17) and (18) [19, 20, 21].

$$\left[\frac{\partial\delta n(x,y,z)}{\partial x}\right]_{x=\pm\frac{g_x}{2}} = \mp\frac{S_g}{Dn(Nb)}\cdot\delta n\left(\pm\frac{g_x}{2},y,z\right) \quad (17)$$

$$\left[\frac{\partial\delta n(x,y,z)}{\partial y}\right]_{y=\pm\frac{g_y}{2}} = \mp\frac{S_g}{Dn(Nb)}\cdot\delta n\left(x,\pm\frac{g_y}{2},z\right) \quad (18)$$

S_g is the recombination velocity at grain boundary; g_x and g_y are respectively the length and the width of the grain.

2.3. Study of the space eigenvalues C_k and C_j

The use of the boundary conditions (17) and (18) gives transcendent equations (19) and (20) whose resolution allows us to obtain the eigenvalues (Ck and Cj) by the graphic method. Keeping gx = gy, the Ck and Cj have the same values [6].

We have opted for the graphical method, where by plotting the function $f(C_k)$ and $h(C_k)$ below, the points of intersection of the two curves yield, the C_k and C_j are obtained in the same way.

$$f(C_k) = \tanh\left(C_k\cdot\frac{g_x}{2}\right) \quad (19)$$

$$h(C_k) = \frac{S_g}{C_k\cdot Dn(Nb)} \quad (20)$$

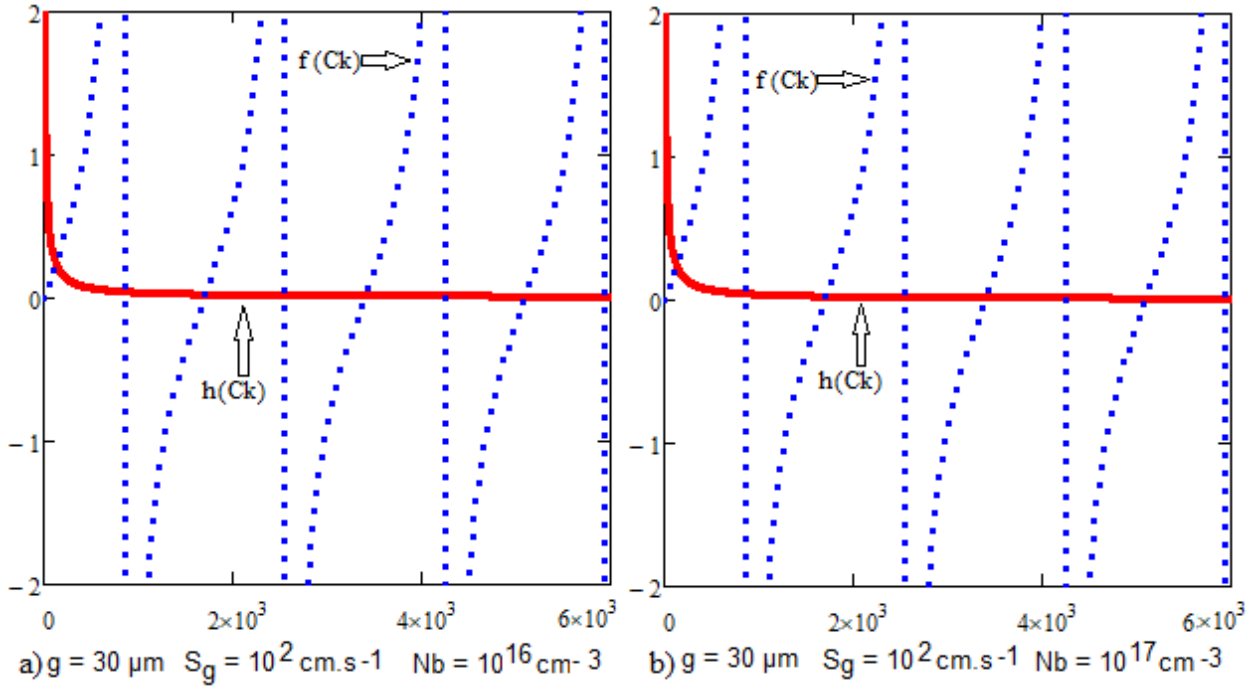

Figure 2: Eigenvalues for $S_g \leq 10^3$ cm.s^{-1}, Nb = 10^{16} cm^{-3}, Nb = 10^{17} cm^{-3}

We note that for $S_g \leq 10^3$ cm.s^{-1} the values of C_k (or C_j) are practically insensitive to the variations of the base's doping rate and the grain boundary recombination velocity (S_g). In the table 1 we noted the values obtained from Figure 2 (a and b):

Table 1: The eigen values C_k for $S_g \leq 10^3$ cm.s^{-1}, g = 30 µm

Base doping rate (cm^{-3})	eigenvalues C_k (cm^{-1}), k =0, 1, 2, 3, and 4				
10^{16}	1699	3397	5095	6793	8491
10^{17}	1699	3397	5095	6793	8491

We checked for several recombination velocity at grain boundary $S_g \leq 10^3$ cm.s^{-1} and whatever the values of the doping rate of the base, C_k (or C_j) values are roughly equal to the values given in Table 1.

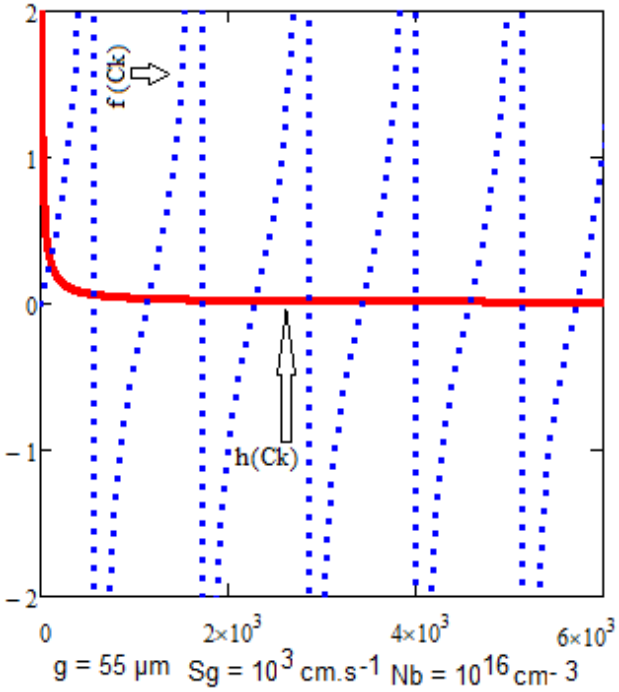

Figure 3: Eigenvalues for $S_g = 10^3$ cm.s^{-1}, Nb = 10^{16} cm^{-3}

Also, grain size has a very large influence on eigenvalues regardless of the grain boundaries recombination velocity and the doping rate of the base. The previous curve was drawn for g= 30 µm. For the curve above (Figure 3) we took g= 55µm; we notice that for the same interval, the number of C_k eigenvalues has almost doubled. This same method allowed us to graphically determine the specific values corresponding to the grain sizes used in this work.

Table 2: eigenvalues (Sg = 10^3 cm.s^{-1}, Nb = 10^{16} cm^{-3}; Dn = 30.37 cm^2.s^{-1})

Sizes (µm)	$C_k = C_j$ (cm^{-1}) ; k= 0, 1, 2, 3, 4				
28	2249	4491	6734	8977	11220
46	1371	2734	4099	5465	6831
55	1148	2287	3429	4571	5713
64	986	1966	2947	3928	4910
73	865	1724	2584	3444	4305
82	771	1535	2300	3066	3832
91	695	1384	2073	2763	3453
100	633	1259	1887	2515	3143

3. Results and Discussions

3.1. Study of the Effective Diffusion Coefficient

The expression of the effective diffusion coefficient [19, 40, 41] as a function of the grain size and grain boundary' recombination velocity and now with the base doping rate, becomes:

$$Dkj\left(S_g, g, Dn(Nb)\right) = \frac{Dn(Nb)\cdot\left[\sin\left(c_k\cdot g_x\right)+c_k\cdot g_x\right]\cdot\left[\sin\left(c_j\cdot g_y\right)+c_j\cdot g_y\right]}{16\cdot\sin\left(c_k\cdot\frac{g_x}{2}\right)\cdot\sin\left(c_j\cdot\frac{g_y}{2}\right)} \qquad (21)$$

In Figure 4, we see a decrease of the effective diffusion coefficient as a function of the doping rate and the grain size. For the low values of the base's doping rate (Nb ≤ 10^{15}cm^{-3}), effective diffusion coefficient is almost constant, so we can say that, the low doping rates of the base have almost noeffect on the effective diffusion of minority excess carriers; however, the influence of the doping rate is significant beyond values above 10^{15} cm^{-3}.

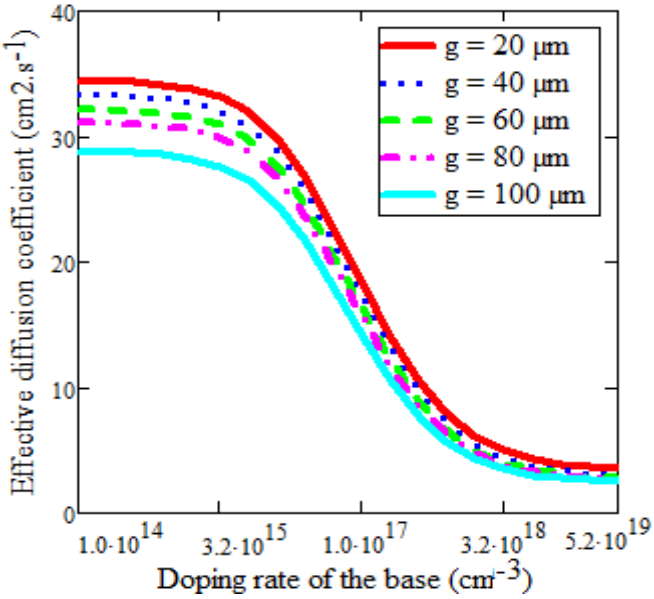

Figure 4: Profile of the effective diffusion coefficient as a function on the doping rate of the base for different grain size; $S_g = 10^3$ cm.s^{-1}.

When the doping rate of the base becomes very high (around 10^{19} cm^{-3}), the effective diffusion coefficient becomes completely independent of the doping rate of the base.

3.2. Study of the minority carrier's density in the base of the solar cell

Doping being one of the stages in the manufacture of solar cells so, it is great interest to know the effect of doping level on the cell efficiency before the cell fabrication.

Thus in this part, as our study carries on a solar cell illuminated by the front face, we have set z = 0 for figures 5, 6, 7; in order to be located at the junction, *Sf* is set to 3.10^3 cm.s^{-1} because: Equation (16) defines the concept of minority carrier junction recombination velocity (*Sf*). *Sf* appears as an effective characteristic of the junction and is related to the solar cell technological parameters: base doping, basewidth… and to the operating conditions (junction polarization). *Sf* quantifies how excess carrier flow through the junction in actual operating conditions and then *Sf* characterizes the junction as an active interface [35, 42]. When *Sf* tends to zero, there is no current flows through the junction so carriers are stored on both sides of the junction: that is the open circuit state of an ideal cell. In a non-ideal cell (real case with losses at the junction), there is a very small current flowing through the junction, which means that an internal load exists in the solar cell: that is the shunt resistance *Rsh* of the cell. This shunt resistance induces an intrinsic junction recombination velocity (*Sf*0) [43, 44], which depends only on the intrinsic parameters of the photovoltaic cell. And *Sb* is the effective back surface recombination velocity. Its value is related to the grain size *g*, the grain boundary recombination velocity *Sg*, the actual value of the intra-grain surface recombination velocity and now with the base doping rate [19, 20, 21]. Its expression is:

$$Sb(H, g, Nb) = D(Nb)\cdot\frac{\sum_{k=0}^{5}\sum_{j=0}^{5}\left(Rkj\left(\frac{D(Nb)}{Lkj}\right)^2\sum_{i=1}^{3}K_i\left[b_i\exp(-b_iH)-b_i\cosh\left(\frac{H}{Lkj}\right)+\frac{1}{Lkj}\sinh\left(\frac{H}{Lkj}\right)\right]\right)}{\sum_{k=0}^{5}\sum_{j=0}^{5}\left(Rkj\left(\frac{D(Nb)}{Lkj}\right)^2\sum_{i=1}^{3}K_i\left[\exp(-b_iH)-\cosh\left(\frac{H}{Lkj}\right)+b_i\cdot Lkj\cdot\sinh\left(\frac{H}{Lkj}\right)\right]\right)} \qquad (22)$$

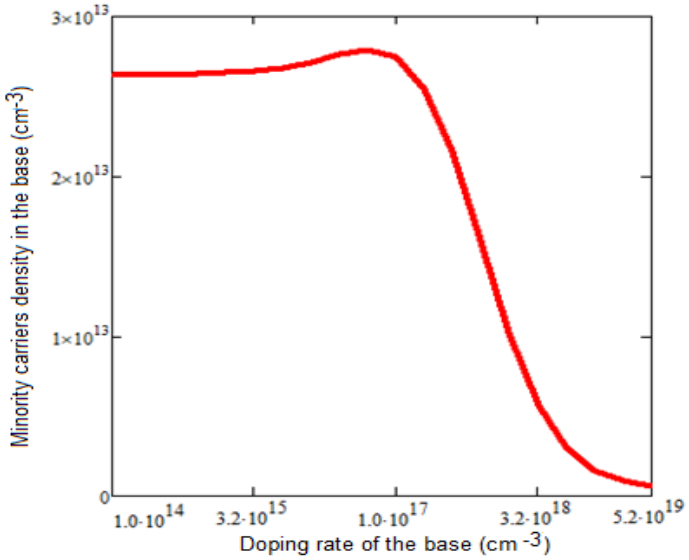

Figure 5: Profile of the excess minority carrier's density in the base as a function of the doping rate of the base: $S_g = 10^3$ cm.s^{-1}, $S_f = 3.10^3$ cm.s^{-1},$S_b = F (N_B)$ cm.s^{-1}, $g_x = g_y = g = 64$ µm, $H = 120$ µm, $z = 0$ µm

Figure 5 shows us that the excess minority carrier's density in the base increases slightly with the doping rate to reach a maximum for a base doping rate equal to $5.12.10^{16}$ cm^{-3}. Above this value, the excess minority carrier's density in the base decreases significantly. Indeed, below $5.12.10^{16}$ cm^{-3}, the increase in the doping rate of the base leads to a slight increase in the minority carriers' density in the base, but above $5.12.10^{16}$ cm^{-3}, the recombination processes are becoming more and more predominant because the diffusion of minority carriers in the base decreases when the doping rate of the base increases, leading to a decrease in the minority carriers density. This variation in the excess minority carriers' density in the base results from the existence of an optimal concentration of doping rate, as can be seen in Figure 5. This optimal doping rate tends to increase due to the increase in grain size (Figure 6). When grain size increases, we notice an increase in the excess carrier density with a shift of maximas of the density of improved carriers in open-circuit in the moderate base doping (10^{15} cm^{-3} ≤ Nb ≤10^{17} cm^{-3}), when we tend to large grain sizes. This phenomenon is explained by the fact that when the grain size is large, recombination rate in the bulk remained less, whatever the grain surface recombination therefore, solar cells with large grains are better than those with small grains [45].

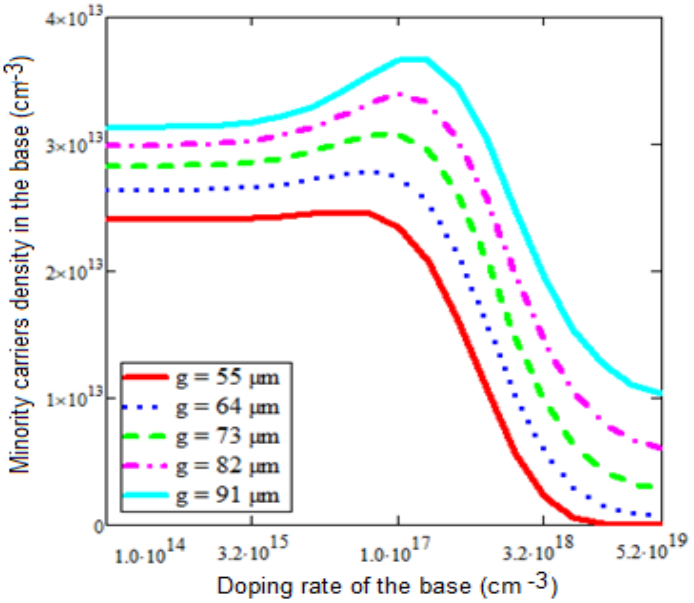

Figure 6: Profile of the excess minority carrier's density in the base as a function of the doping rate of the base for different grain sizes: $S_g = 10^3$ cm.s^{-1}, $S_f = 3.10^3$ cm.s^{-1}, $S_b = F (N_B, g)$ cm.s^{-1}, $H = 120$ µm, $z = 0$ µm.

For the value of a given size, the optimal doping rate is obtained when the minority carrier's density in the base reaches its maximum of the excess minority carriers density of improved (δn_{max}) in open-circuit in the moderate doping; thus we give Table 3 the optimal doping rate values for different grain sizes and the maximum of the excess minority carriers density of improved (δn_{max})**.**

Table 3: Maximum of the excess minority carrier's density of improved carriers (δn_{max}) in open-circuit in the moderate base doping (10^{15} cm^{-3} ≤ Nb ≤10^{17} cm^{-3}) and optimal doping rate for different grain sizes obtained by the graph method

Grain size in cm	0,0055	0,0064	0,0073	0,0082	0,0091
Base optimal doping rate Nb_{opt} in cm^{-3}	2,86. 10^{16}	5 ,12.10^{16}	7,38.10^{16}	10^{17}	1,124.10^{17}
δn_{max} ins cm^{-3}	2,467.10^{13}	2,7889.10^{13}	3,0853.10^{13}	3,3898.10^{13}	3,667.10^{13}
Ln (Size)	-5,2030072	-5,0514573	-4,9198809	-4,8036211	-4,7105307
Ln (Nb_{opt})	37,8921831	38,4745159	38,8401351	39,1439466	39,8608403
Ln (δn_{max})	30,836609	30,9592535	31,0602551	31,1543771	31,2329801

Based on the results obtained in the table (3), we represented in Figure 7 the curve of the logarithm of the maximum of excess minority carrier's density according to the logarithm of the grain size (a) and the logarithm of optimal doping rate of the base (b).

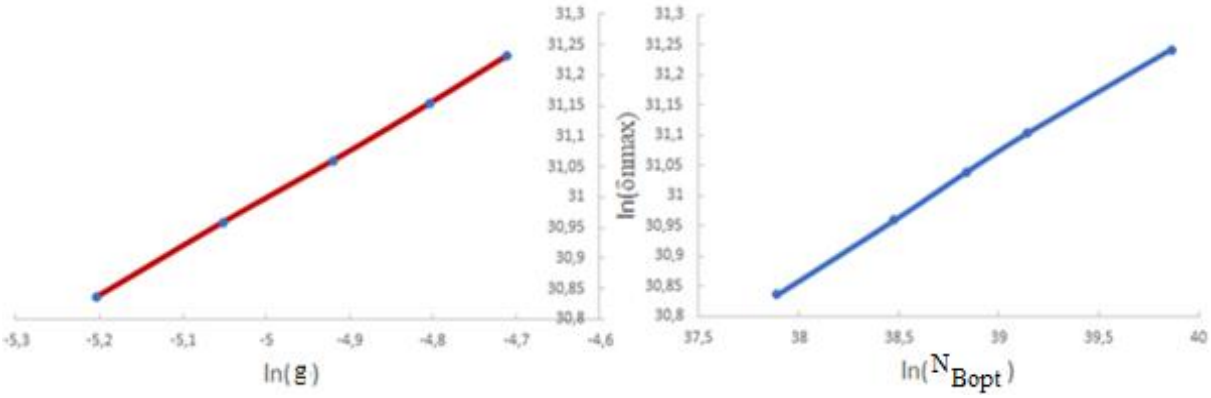

Figure 7: logarithm of the maximum excess minority carrier density (Z = 0 µm, Sf = 3.10^3 cm.s^{-1}) as a function of the
a) logarithm of grain size
b) logarithm of optimal doping rate

These curves allow us to write the following relationships:

$$Ln\delta n\max = a_1 \cdot \ln g + \ln b_1 \quad (21)$$

$$Ln\delta n\max = a_2 \cdot \ln Nb_{opt} + \ln b_2 \quad (22)$$

The equations (21 and 22) allows us to obtain the optimal doping rate of the base according to the grain size.

$$Nb_{opt}(g) = \sqrt[0.936307883]{2.09955379 \cdot 10^{11} \cdot g^2} \quad (23)$$

4. Conclusion

In this work, we have given the expression of the excess minority carrier's density according to the doping rate and grain size. Then, from on its profile versus on the doping rate for different grain size values, the optimal doping rate corresponding to the maximum of the excess minority carrier's density of improved carriers (δn_{max}) in open-circuit in the moderate base doping (10^{15} cm^{-3} ≤ Nb ≤10^{17} cm^{-3}) for each grain size value is deducted. We then established a relationship that dregs the optimal doping rate with grain size.

References

[1]. Martin A. Green, Keith Emey, Yoshihiro Hishikawa and Wilhelm Warta (2011). Solar cell efficiency tables (version 37). Prog Photovolt: Res. Appl. N0 19, pp 84-92. (Willey). DOI: 10. 1002/pip. 1088

[2]. Bester, Y., Ritter, D., Bahia, G., Cohen, S. and Sparkling, J. (1995). Method Measurement of the Minority Carrier Mobility in the Base of Heterojunction Bipolar Transistor Using a Magneto transport Method. Applied Physics Letters, 67, 1883- 1884. https://doi.org/10.1063/1.114364

[3]. G. E. Ayvazian, G. H. Kirakosyan and G. A. Minasyan. (2004). Characteristics of Solar Cells with Vertical p-n Junction. Proceedings of 19th *European Photovoltaic Solar Energy Conference, Paris*, 7-11 June 2004, pp117-119.

[4]. I. Diatta, I. Ly, M. Wade, M. S. Diouf, S. Mbodji, and G. Sissoko. (2016). Temperature Effect on Capacitance of a Silicon Solar Cell under Constant White Biased Light World. *Journal of Condensed Matter Physics*, 6, pp261-268
http://www.scirp.org/journal/wjcmp

[5]. Y. Traore, N. Thiam, M. Thiame, A Thiam, M. L. Ba, M. S. Diouf, I. Diatta, O. Mballo, El H Sow, M. Wade and G. Sissoko, (2019), AC Recombination Velocity in the Back Surface of a Lamella Silicon Solar Cell under Temperature. *Journal of modern physics*, pp.1235-1246

[6]. A. M. M. Kosso, M. Thiame, Y. Traore, I. Diatta, M. Ndiaye, L. Habiboullah, I. Ly, G. Sissoko, (2018). 3D Study of a Silicon Solar Cell under Constant Monochromatic Illumination: Influence of Both, Temperature and Magnetic Field. *Journal of Scientific and Engineering Research*, 5(7), pp.259-269

[7]. R. Mané, H. L. Diallo, H. Y. Ba, I. Diatta, Y. Traoré, Ch. T. Sarr and G. Sissoko, (2018), Influence of both magnetic field and temperature on silicon solar cell photogenerated current, *Journal of scientific and engineering research*, pp. 2394-2630

[8]. N. M. M. O. Mohamed, O. Sow, S. Gueye, Y. Traore, I. Diatta, A. Thiam, M. A. Ba, R. Mane, I. Ly and G. Sissoko, (2019), Influence of Both Magnetic Field and Temperature on Silicon Solar Cell Base Optimum Thickness Determination, *Journal of modern physics*, pp. 1596-1605

[9]. T. Sumita, M. Imaizumi, S. Matsuda, T. Ohshima, A. Ohi and H Itoh. (2003) Proton radiation analysis of multi-junction space solar cells. *Nuclear Instruments and Methods in Physics Research*, B206, pp 448–451.

[10]. O. Sow, M. L. Ba, H. Y. Ba, M. A. O. El Moujtaba, Y. Traore, M. S. Diop, H. Lemrabott, M. Wade, G. Sissoko, (2019), Shunt Resistance Determination in a Silicon Solar Cell: Effect of Flow Irradiation Energy and Base Thickness, *Journal of electromagnetic Analysis and Application*, pp. 203-216.

[11]. Nzonzolo, D., Lilonga-Boyenga, Sissoko, G. (2014) Illumination Level Effects on Macroscopic Parameters of a Bifacial Solar Cell. Energy and Power Engineering, 6, pp. 25-36.

[12]. H. Y.BA, B. Seibou, I. Gaye, I. Ly and G. Sissoko. (2014) Recombination Parameters Measurement of Silicon Solar Cell under Constant White Bias Light with Incident Angle Current. *Trends in Technology and Sciences*, 3, 411-415.

[13]. O. Diasse, A. Diao, M. Wade, M. S. Diouf, I. Diatta, R. Mane, Y. Traore, and G. Sissoko, (2018). Back Surface Recombination Velocity Modeling in White Biased Silicon Solar Cell Under Steady State. *J. Mod. Phys*. 9, pp.189-201.

[14]. M.L.O. Cheikh, B. Seibou, M. A. O. Moujtaba, K. Faye, M. Wade and G. Sissoko. (2015) Study of Base Doping Rate Effect on Parallel Vertical Junction Silicon Solar Cell under Magnetic Field. *International Journal of Engineering Trends and Technology*, 19, *pp44-55.*

[15]. M. S. Diop, H. Y. Ba, Nd. Thiam, I. Diatta, Y. Traoré, M. L. Ba, El. Sow, O. Mballo, G. Sissoko (2019). Surface Recombination concept as applied to determinate silicon solar cell base optimum thickness with doping level effect. World Journal of Condensed Matter Physics, 9, pp.102-111
https://doi.org/10.4236/wjcmp.2019.94008

[16]. Mats Rosling, Henry Bleichner, Mans Mundqvist and Edvard Nordlander (1992). A Novel Tehcnical for the Simultaneous Measurement of Ambipolar Carrier Lifetime and Diffusion Coefficient in Silicon, Solid-State Electronics, Vol. 35, Issue 9, pp1223-1227.

[17]. K. Misiakos, C. H. Wang, A. Neugroschel and F. A. Lindholm (1990). Simultaneous extraction of minority carrier parameters in crystalline semiconductors by lateral photocurrent, *J.Appl. Phys.* 67(1): pp321-333

[18]. M. Rugider, T. Puzzer, E. Schäffer, W. Warta, S. W. Glunz, P. Würfel, T. Trupke (2007). Diffusion lengths of silicon solar cells frop luminescence images. 22nd *European Photovoltaic Solar Energy Conferences.* 3-7, p. 309

[19]. H. L. Diallo, A. S. Maiga, A. Wereme, G. Sissoko, (2008). New Approach of Both Junction and Back Surface Recombination Velocity in a 3D Modelling Study of a Polycrystalline Silicon Solar Cell. *Eur. Phys. J. Appl. Phys*. 42, pp.203-211

[20]. O. Mbao, M. Thiame, I. LY, I. Datta, M. S. Diouf, Y. Traore, M. Ndiaye and G. Sissoko, (2016). 3D Study of a Polycrystalline Bifacial Silicon Solar Cell, Illuminated Simultaneously by Both Sides: Grain Size and Recombination Velocity Influence. *International Journal of Innovative Science, Engineering & Technology*, Vol. 3 Issue 12, pp.152-162.

[21]. M. Thiame, A. Diene, B. Seibou, Ch. T. Sarr, M. L. O. Cheikh, I. Diatta, M. Dieye, Y. Traoré, G. Sissoko, (2017). 3D Study of a Bifacial Polycrystalline Silicon Solar Cell Back Surface Illuminated: Influence of Grain Size and Recombination Velocity, *Journal of Scientific and Engineering Research*. 4(1) pp 135-145.

[22]. J. Zhao, A. Wang, P.Altematt, M. A. Green, Progress in Photovoltaic. **7,** 47 (1999).

[23]. P.P. Altermatt, J.O. Schumacher, A.Cuevas, S.W. Glunz, R.R. King, G. Heiser, A. Schenk, *Proceedings of the16th European Photovoltaic Solar Energy Conference, Glasgow, UK, 1-5* (2000) pp. 102-105

[24]. H. El Ghatani and S. Martinuzzi, (August 1989). Influence of Dislocation on Electrical Properties of Large Grained Polycrystalline Silicon Cells. *I. Model. J. Appl. Phys*. 66(4), 15, pp.1717-1722.

[25]. S. R. Dhariwal, (1988). Photocurrent and Photovoltage from Polycrystalline p-n Junction Solar Cells, Vol.25. pp 223-233.

[26]. J. Dugas, (1994). 3D Modelling of a Reverse Cell Made With Improved Multicrystalline Silicon Wafers. Solar Energy Materials and Solar Cells 32, pp.71-88.

[27]. M. Dieye, S. Mbodji, M. Zoungrana, I. Zerbo, B. Dieng, G. Sissoko, (2015). A 3D Modelling of Solar Cell's Electric Power under Real Operating Point. *World Journal of Condensed Matter Physics*, 5, pp.275-283.

[28]. M. Saritas and H. D. Mckell, (1988). Comparison of Minority-Carrier Diffusion Length Measurements in Silicon by the Photoconductive Decay and Surface Photovoltage Methods, *J. Appl. Phys.* 63 (9), pp4561-4567.

[29]. H.S. Rauschenbach, (1980) Solar Cell Array Design Handbook. The Principles and Technology of Photovoltaic Energy Conversion (Van Nostrand Reinhold Ltd., New York,1980)

[30]. M. M. Dione, A. Diao, M. Ndiaye, H. L. Diallo, N. Thiam, F. I. Barro, M. Wade, A. S. Maiga. G. Sissoko, (2010). 3D Study of Monofacial Silicon Solar Cell Under Constant Monochromatic Light: Influence of Grain Size Grain Boundary Recombination Velocity, Illumination Wavelength Back Surface and Junction Recombination Velocities: Proceeding of 25th *European Photovoltaic Solar Energy Conference and Exhibition 5th World Conference on Photovoltaic Energy Conversion* pp. 488-491.

[31]. J. Furlan, and S. Amon, (1985) Approximation of the carrier generation rate in illuminated silicon. Solid State Electron, 28, pp. 1241–43.

[32]. S. N. Mohammad, (1987). An Alternative Method for the Performance Analysis of Silicon Solar Cells, *J. Appl. Phys.*, LXI (2), pp. 767-772.

[33]. J. G. Fossum, (1976) Computer aided numerical analysis of silicon solar cells solid-state electronics, 19, pp.269-277. doi.org/10.1016/0038-1101 (76)90022-8

[34]. J. G. Fossum and D. S. Lee (1952). A physical model for the dependence of carrier life time on doping density in non-degenerate silicon solid-state electronics, 15, pp.741-747. doi.org/10.1016/0038-1101 (82)90203-9

[35]. G. Sissoko, E. Nanema, A. Correa, M. Adj, A.L. Ndiaye, M.N. Diarra, (1998). Recombination Parameters Measurement in Double Sided Surface Field Solar Cell Proceedings of World Renewable Energy Conference, Florence–Italy, pp.1856-1859.

[36]. G. Sissoko, C. Museruka, A. Correa, I. Gaye and A. L. Ndiaye, (1996). Light Spectral Effect on Recombination Parameters of Silicon Solar Cell', Proceedings of the World Renewable Energy Congress, Denver-USA, Part III, pp.1487-1490.

[37]. F.I. Barro, I. Zerbo, O.H. Lemrabott, F. Zougmore, G. Sissoko. (2001). *Proceedings of the 17th European Photovoltaic Solar Energy Conference and Exhibition* Munich Germany, pp 368-371

[38]. M. M. Dione, I. Ly, A. Diao, S. Guéye, M. Thiame, G. Sissoko, (2013). Determination of the Impact of Grain Size and the Electrical Parameters of a Bifacial Polycristallin Silicium Solar Cell. *Engineering Science and Technology: International Journal* Vol. 3, N° 1; pp. 66-73

[39]. S.M. Sze (1981) Physics of semiconductor Devices, 2nd Edition, Wiley Interscience, New York.

[40]. J. Oualid, M. Bonfils, J P Crest G. Mathian H Amzil, J. Dugas, M. Zehaf and S. Martinuzzi. (1982). Photocurrent and Diffusion Lengths at the Vicinity of Grain Boundaries (g.b.) in N and P-type Polysilicon. Evaluation of the g.b. Recombination Velocity RevuePhys. Appl. 17, pp119-124

[41]. C. Donolato. (1999). Effective Diffusion Length of Multicrystalline Solar Cells. *Solid State Phenomena*. 67-68, pp75-80.

[42]. B. Ba, M. Kane, A. Fickou, and G. Sissoko. (1995). Open-circuit Voltage Decay in Polycrystalline Silicon Solar Cells. *Energy Materials and Solar Cells*. 31**,** 1, pp 259-271.

[43]. G. Sissoko, E. Nanema, A. Correa, P. M. Biteye, M. Adj, A. L. Ndiaye, (1998). *Proceedings of the World Renewable Energy Conference Florence- Italy*, pp.1848 - 1851.

[44]. A. Rohatgi, S. Narasimha, D.S. Ruby.(1998) *Proceedings of the 2nd World Conference and Exhibition on Photovoltaic Solar Energy Conversion*, Stephens, Bedford pp.1566-1569.

[45]. M.C. Halder and T.R. Williams. (1983). Grain boundary effects in polycrystalline silicon solar cells II: numerical calculation of the limiting parameters and maximum efficiency. Solar Cells, Vol. 8, pp 201-223.